

Second Harmonic Generation of Nanoscale Phonon Wave Packets

A. Bojahr,¹ M. Gohlke,¹ W. Leitenberger,¹ J. Pudell,¹ M. Reinhardt,² A. von Reppert,¹ M. Roessle,¹
M. Sander,¹ P. Gaal,² and M. Bargheer^{1,2,*}

¹Institut für Physik und Astronomie, Universität Potsdam, Karl-Liebknecht-Strasse 24-25, 14476 Potsdam, Germany

²Helmholtz Zentrum Berlin, Albert-Einstein-Strasse 15, 12489 Berlin, Germany

(Received 1 June 2015; published 5 November 2015)

Phonons are often regarded as delocalized quasiparticles with certain energy and momentum. The anharmonic interaction of phonons determines macroscopic properties of the solid, such as thermal expansion or thermal conductivity, and a detailed understanding becomes increasingly important for functional nanostructures. Although phonon-phonon scattering processes depicted in simple wave-vector diagrams are the basis of theories describing these macroscopic phenomena, experiments directly accessing these coupling channels are scarce. We synthesize monochromatic acoustic phonon wave packets with only a few cycles to introduce nonlinear phononics as the acoustic counterpart to nonlinear optics. Control of the wave vector, bandwidth, and consequently spatial extent of the phonon wave packets allows us to observe nonlinear phonon interaction, in particular, second harmonic generation, in real time by wave-vector-sensitive Brillouin scattering with x-rays and optical photons.

DOI: 10.1103/PhysRevLett.115.195502

PACS numbers: 62.25.-g, 63.20.-e, 78.20.hc, 78.47.J-

Basic physics lectures introduce phonons as uncoupled quanta of the lattice excitation, i.e., delocalized quasiparticles with certain energy and momentum. The low-temperature heat capacity of insulators and blackbody radiation are fundamental macroscopic consequences of quantum mechanics. Anharmonic effects are introduced to discuss heat expansion and thermal transport, where only thermally activated phonons contribute to these phenomena. Typically, theory averages over thermally excited quantum states before properties of the “mean heat carrying phonon” are compared to macroscopic measurements like the temperature of a solid. Our Letter shows a route towards detailed experimental information on mode-specific nonlinear interactions. This will facilitate fundamental tests of the theory avoiding the calculation of thermal averages, which inevitably obscure the full information.

Such progress is of high relevance for the “hot topic” of heat transport manipulation in nanostructures which is driven by the enormous size reduction of integrated circuits [1–6] and the field of thermoelectrics. Recent work aims at improving the conversion of waste heat into usable energy by tailored phonon-phonon interaction processes [7–9]. Nonlinear effects have been predicted to yield efficient thermal diodes [10]. Only in a few cases has the full phonon dispersion relation including the linewidth (inverse lifetime) been measured by inelastic scattering [11–13], and at low wave vectors the instrumental resolution currently sets limits. Linewidth measurements yield mode-averaged dissipation, but experimental knowledge about the dominant coupled modes is unavailable. The free-electron lasers hold great promise to access the coupling in the femtosecond time domain using diffuse scattering and inelastic x-ray scattering [14,15]. Recently, the coupling of terahertz excited optical phonons with other optical phonons was

observed and presented as one example of nonlinear phonon interactions [16].

Nonlinear phononics as discussed here shows many analogies to nonlinear photonics in transparent media where high electromagnetic wave fields yield nonlinear polarizations. These processes are described by interacting photons that fulfill momentum and energy conservation. The description of these optical phenomena is robust and extremely well tested by an enormous number of experiments such as sum- and difference-frequency generation or four-wave mixing. The first analogous experiments on nonlinear phononics date back to the 1960s, when collisions of two ultrasound beams were studied in real time and space [17]. These experiments somewhat resembled nonlinear optics before the utilization of the laser. The required interaction volume was in the centimeter range, and the time resolution was limited by the 10 MHz ultrasound frequency. The phonon analogue of optical supercontinuum generation by femtosecond lasers was studied in seminal picosecond-ultrasonics experiments on the self-steepening of the strain-pulse fronts [18,19] which finally lead to acoustic solitons [20–22]. In these experiments, the excitation of nanometric strain waves was not wave-vector specific. Recent progress in the creation and detection of gigahertz and terahertz phonon wave packets also known as hypersonic strain waves makes them a perfect test ground to investigate phonon-phonon interaction processes on the nanoscale [23].

In this work, we combine the selective excitation of longitudinal acoustic phonon wave packets with time-resolved variants of x-ray and broadband Brillouin scattering [23] to investigate the nonlinear interaction of phonons with a specific wave vector. The experiments provide a high temporal and spatial resolution for observing phonon dynamics in real time over a broad range of wave vectors which

correspond to the nanometer length scale. As the basic example of nonlinear phononics, we shaped giant and ultra-short phonon wave packets with well-defined momenta and observed the generation of their second harmonic (SH).

To create such giant amplitude strain waves, ultrashort laser pulses excite a metallic strontium ruthenate (SRO) film deposited on a bulk strontium titanate (STO) substrate, a system where we know the first-order lattice anharmonicity [19] and where the acoustic impedances of the thin film and substrate are nearly matched [24]. The metal film expansion induced by each laser pulse launches a bipolar strain pulse into STO [24]. A train of several laser pulses [Fig. 1(b)] with a defined temporal delay τ creates a phonon wave packet with a fundamental frequency of $\Omega = 2\pi/\tau$ [23,25,26]. If the laser-pulse train is composed of femtosecond pulses (blue lines in Fig. 1), the phonon wave packet exhibits

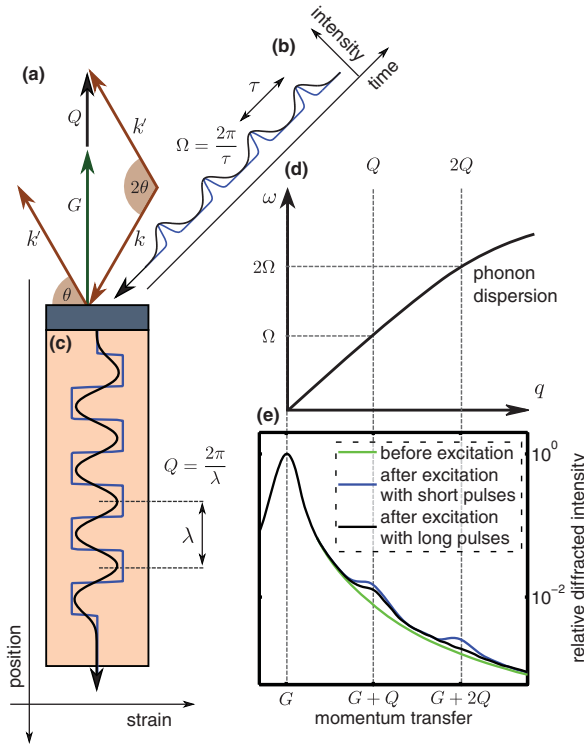


FIG. 1 (color). Preparation and observation of phonon wave packets. (a) X-rays with wave vector k are scattered (k') by the reciprocal lattice vector G plus a phonon with wave vector Q . (b) A metal film is excited by a laser-pulse train with short (blue) and long (black) pulses. (c) Short pulses excite phonon wave packets at the fundamental and higher harmonics [rectangular wave packet (blue)]. Excitation with long pulses suppresses higher harmonics and generates a sinusoidal wave (black). (d) The phonon dispersion relation connects the central frequency $\Omega = 2\pi/\tau$ of the excited phonon wave packet with its corresponding wave vector $Q = 2\pi/\lambda$. (e) Experimental data of ultrafast x-ray diffraction from the unexcited sample shows the (002) substrate reflection (green). After excitation with short pulses (blue), peaks at $G \pm Q$ and $G \pm 2Q$ occur. These peaks originate from inelastic scattering by the induced phonon wave packet. For longer pump pulses (black), the scattering at $G \pm 2Q$ is suppressed. This evidences that a narrow band phonon wave packet without its higher harmonics was excited.

several sharp strain fronts [Fig. 1(c)], corresponding to the excitation of higher harmonics $n \cdot \Omega$. These harmonics are identified in ultrafast x-ray diffraction (UXRD) experiments from their wave vector Q according to the dispersion relation of longitudinal phonons [$\omega = v_L q$, plotted in Fig. 1(d)]. For small wave vectors, $v_L(q)$ is a constant describing the longitudinal sound velocity. The UXRD data in Fig. 1(e) were obtained with an ultrathin SRO transducer layer ($d = 15$ nm). The green curve displays the relative diffraction intensity before the four pump pulses ($\tau = 11$ ps) reach the sample. The peak at G corresponds to the reciprocal lattice vector (002) of the STO substrate. When the 100 ps x-ray pulse was probing the sample shortly after the generation of the wave packet, additional diffraction intensity at $G \pm Q = n \cdot 0.071$ nm $^{-1}$ was detected (blue curve). The diffraction intensity is a direct measure of the spectral energy distribution of the imprinted coherent phonon modes [27]. When we increased the width of the pump pulses from $\Delta\tau_{\text{FWHM}} = 0.9$ to 3.4 ps, the diffraction of higher orders of Q was suppressed and we observed only the additional scattering from $G \pm Q$ (black curve) as suggested by the wave vector diagram in Fig. 1(a). High-frequency components of an oscillator can be excited only by stimuli which contain these frequencies.

To demonstrate second harmonic generation (SHG) of monochromatic phonon wave packets, we repeated the UXRD experiment with a 70 nm SRO transducer, which absorbs more optical energy. We used only two long laser pulses ($\tau = 17.7$ ps and $\Delta\tau_{\text{FWHM}} = 5.3$ ps) while keeping the total incident laser fluence constant. This doubles the local atomic displacement and quadruples the acoustic energy density $\mathcal{E} = E/V$ of the wave packet in the volume V —defined by the beam area and the length of the wave packet. This increased the up-conversion efficiency of phonons at the expense of monochromaticity according to the higher wave packet localization in space.

Figure 2(a) shows the fundamental phonon peak around $Q = 0.044$ nm $^{-1}$ which was observed in the UXRD experiment when the x-rays probed the sample immediately after excitation. For time delays around 200 ps, a tiny peak at $2Q = 0.088$ nm $^{-1}$ occurred. This rising SH is enhanced in Fig. 2(b), where the measured diffraction signal is multiplied by q^2 for better visibility. Figure 2(c) quantifies the transient change of the peak area Σ_i in the vicinity of 0.044 and 0.088 nm $^{-1}$ [28]. $\Sigma_i \sim \mathcal{E}_i$ is proportional to the energy density $\mathcal{E}_i \sim \int \rho_E(q, t) dq$ of the phonons around $q = iQ$, obtained from integrating the spectral energy density $\rho_E(q, t)$ over the bandwidth of the fundamental ($i = 1$) and the SH ($i = 2$), respectively [27].

The signal Σ_1 of the excited fundamental mode (red diamonds) increased immediately after excitation, followed by a nearly exponential decay. Σ_2 describing the SH (cyan dots) was delayed by approximately 200 ps. Thus, the SH was not directly excited by the laser pulses but was only generated by the propagation of phonons in the anharmonic lattice of STO. The delay was longer than the 100 ps time

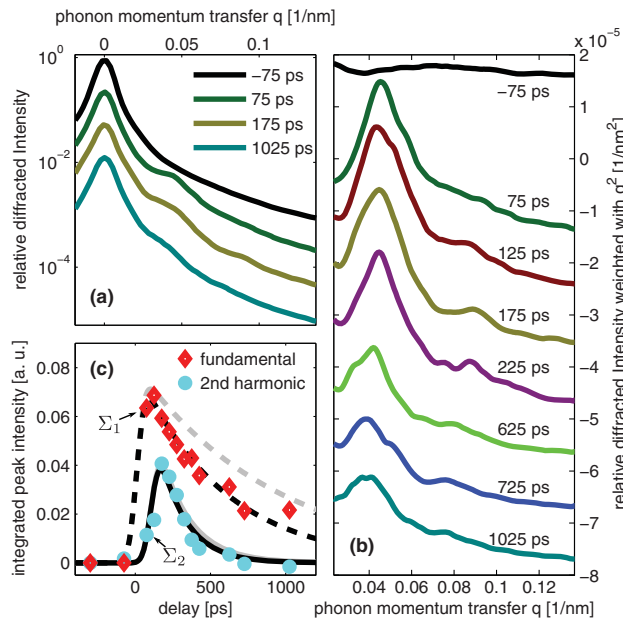


FIG. 2 (color). Transient x-ray diffraction from photoexcited phonons and their SH. (a) X-ray diffraction signals around the (002) lattice plane of the STO substrate. (b) Diffraction signals on the right shoulder of the STO substrate peak weighted by q^2 for better visualization. The peak around $Q = 0.044 \text{ nm}^{-1}$ after time zero reflects the optically excited coherent phonon wave packet with the central wave vector Q . After a delay of 200 ps, additional diffraction intensity around $2Q$ heralds the SH of Q generated via anharmonic phonon phonon interaction. (c) The gray (black) lines quantify the transient change of the integrated peak intensities of the fundamental and its second harmonic with (and without) a correction for the x-ray absorption.

resolution of this synchrotron experiment [37] and is a direct evidence for the SHG of phonons. Although the SH is continuously generated, it reaches its maximum very fast, since the damping of phonons scales with the square of the frequency.

The SH phonons damped out faster than the fundamental as expected for the frequency dependence of the damping rate $\Gamma \sim \omega^2$ [27]. The gray lines in Fig. 2(c) show the damping of both phonons corrected for effects of x-ray absorption in STO [27]. The corrected exponential decay times for the fundamental and the SH are 1056 and 300 ps, respectively, in good agreement with the literature values [27,38].

To confirm our result and to explore the SHG of phonons in the same sample in more detail, we performed broadband time-domain Brillouin-scattering (TDBS) experiments, which measure a substantial fraction of the phonon spectrum from 0.035 to 0.06 nm^{-1} in STO [23]. We set the pulse separation to $\tau = 30 \text{ ps}$ to let the SH phonon emerge at $2Q = 0.052 \text{ nm}^{-1}$, in the center of the spectrum accessible by TDBS. The black line in Fig. 3(a) shows the time-dependent optical reflectivity change at $\lambda = 580 \text{ nm}$ which corresponds to this wave vector. The reflectivity increases in two steps from the two-pulse heating of SRO. We define the time zero as 7.5 ps after the maximum of the second pump pulse, confirmed by optical cross-correlation. The amplitude

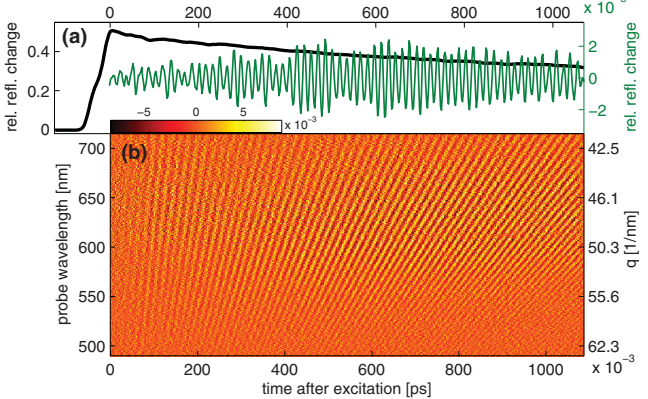


FIG. 3 (color). SHG of phonons observed by TDBS. (a) Transient relative reflectivity change at 580 nm (black line). The stepwise increase indicates the laser excitation of the metal film terminating at $t = 0$. Superimposed reflectivity oscillations (green line) originate from the SH phonons. The oscillation amplitude grows with the number of phonons up-converted to their SH. (b) Measured reflectivity oscillations across the white light probe spectrum. For each wavelength, the oscillation amplitude measures the occupation of a certain phonon q .

of the small superimposed oscillations with the phonon period 2Ω are a measure of how many second-harmonic phonons are present in the sample [23,39]. The rising oscillation amplitude indicates the nonlinear phonon interaction generating the SH of Q . The green line in Fig. 3(a) shows almost no SH phonons just after the two pump pulses with a pulse width of $\Delta\tau_{\text{FWHM}} = 15 \text{ ps}$. The maximum number of these phonons is observed after approximately 600 ps. In the UXRD data of Fig. 2(c), the maximum is observed earlier, because the phonons with larger wave vector $Q = 0.088 \text{ nm}^{-1}$ suffer a much stronger damping.

The broadband detection scheme allowed us to evaluate the spectral content of this SH phonon wave packet even more precisely. The relatively broad wave vector spectrum that extends over a large fraction of the visible range [Fig. 3(b)] results from the spatial confinement of the excited strain wave to two oscillation cycles [23]. We extracted the oscillation amplitude $a(q, t)$ of the relative reflectivity change as a function of the time delay for each probe wavelength λ corresponding to the different wave vectors q which compose the wave packet in the vicinity of $2Q$ [28–36,40].

In these experiments, the spectral energy density of the acoustic wave packet $\rho_E(q, t)$ is proportional [39] to the square of the reflectivity modulations $a(q, t)^2$ divided by q^2 : $\rho_E \sim a(q, t)^2/q^2$. The experimentally derived energy proportional quantity $a(q, t)^2/q^2$ is plotted in Fig. 4(a) as contour lines and compared to the transiently changing spectral energy density $\rho_E(q, t)$ calculated on the basis of a Fermi-Pasta-Ulam (FPU) α - β chain with an empirical damping term. The FPU chain is widely used in theory to investigate phonons in the nonlinear lattice as well as heat transport in 1D [41–44]. In fact, we simulated a chain of oscillators with masses describing SRO and STO

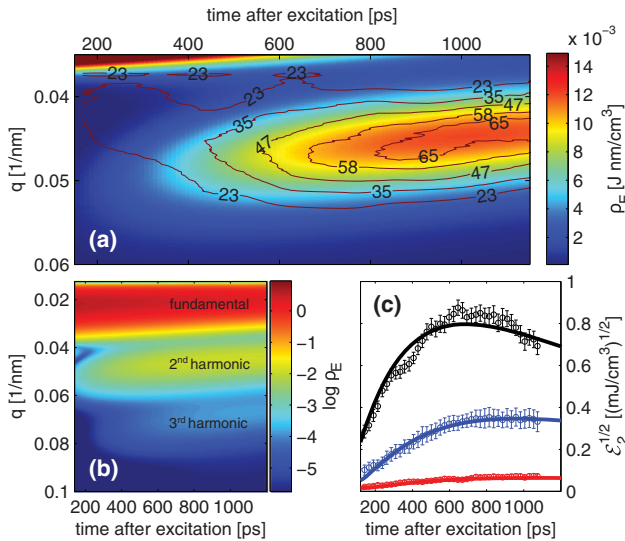


FIG. 4 (color). Comparing SHG experiments to the theory. (a) The color code shows the calculated transient change of the spectral energy density ρ_E around the SH of the excited phonons. The square of the measured relative reflectivity oscillation amplitude divided by q^2 in units of 10^{-7} nm $^{-2}$ is overlaid as contour lines. (b) Calculated ρ_E over a broader range of wave vectors in the log scale. The photoexcited fundamental is transformed into the second and third harmonics. (c) visualizes the measured transient energy density change of the SH for different initial energy densities E_1 (red = 13, blue = 67, and black = 235 nJ/cm 3) of the wave packet and compares this with theoretical calculations (solid lines). The wave vector for the highest energy density was $q = 0.03$ nm $^{-1}$, somewhat larger than the $q = 0.025$ nm $^{-1}$.

unit cells connected by anharmonic springs, where the second-order elastic constants along the [001] direction were derived from the speed of sound determined by time-resolved measurements [19,24,28]. From the comparison of the experimental data to the simulation, we found a third-order elastic constant describing the lattice anharmonicity in STO $C_{111} = -3.9 \times 10^{12}$ N/m 2 consistent with single-pulse time-resolved Brillouin scattering experiments [19]. It is 20% smaller than the value measured by megahertz acoustics at a frequency which is 3 orders of magnitude smaller [45]. In the calculation, the first few oscillators representing the opaque SRO film experience quasi-instantaneous [46] forces which describe the ultrafast heating by the two laser pulses. The force amplitude is known from previous UXRD measurements of the ultrafast lattice dynamics of SRO films [24].

Figure 4(b) shows $\rho_E(q, t)$ on a logarithmic scale over a broader wave vector range. The fundamental mode at 0.025 nm $^{-1}$ is indeed excited at $t = 0$ ps, and subsequently phonons at the second and third harmonics are generated. The second harmonic is generated earlier than the third harmonic. This is an intrinsic feature of this linear chain calculation. By considering only the third order of the lattice potential as the nonlinear term, only three phonon

processes are allowed [47,48], and the third harmonic can only be generated via two sequential scattering processes. By observing the very weak third-harmonic generation, one could get information about the importance of higher orders of the lattice potential.

A pronounced feature of the measured data is the slow shift of the spectral distribution towards smaller wave vectors. The physical origin is uncovered by the simulations which show that the compressive strain front travels faster than the expansive strain. Since the wave packet contains only two strain cycles, this leads to a slightly increasing central wavelength of the wave packet [19,28]. This effect is much less pronounced for wave packets with more cycles.

Finally, the solid lines in Fig. 4(c) show the square root of the energy density \mathcal{E}_2 of the generated SH as a function of time for three different initial energy densities E_1 of the excited fundamental mode. The initial linear increase and the linear dependence $\sqrt{\mathcal{E}_2} \sim E_1$ are characteristic for this second-order nonlinear process of sum frequency generation or three-phonon scattering in general [48]. The corresponding experimental data obtained from integrating $a(q, t)^2/q^2$ over the same wave vector range show excellent agreement. Both the experimental and simulated energy density in Fig. 4(c) take into account that, for the same total energy deposited, the energy density is larger for higher wave vectors. To achieve the highest energy density, it was necessary to increase the wave vector to $q = 0.03$ nm $^{-1}$ in order to avoid multishot damage of the sample.

Conclusion.—With the generation of the SH of a certain well-defined phonon wave packet, we have demonstrated a first conceptually simple experiment that monitors an elementary process of nanoscale nonlinear phononics in real time. The observed damping of the fundamental and SH to other modes is proportional to the square of the wave vector. We strongly believe that these experiments stimulate a series of new experiments ranging from simple extensions such as difference-frequency mixing to more complex experiments which are analogs of four-wave mixing, well known in experimental photonics. Future investigations may address the coupling of optical phonons to acoustic phonons and extend the phase-matching considerations by including also transverse polarisation of phonons and by going to larger wave vectors where the dispersion relation is bending over. Improvements of the signal-to-noise ratio may eventually permit studies on the single quantum level. A similar stimulus may be expected for theory. The Fermi-Pasta-Ulam chain can well predict effects related to longitudinal phonons. Modeling anharmonic phonon propagation and interaction in three dimensions including longitudinal and transverse phonon polarization in detail remains a major challenge. Exploring the physical nature of phonon damping processes and describing soft mode behavior in the vicinity of structural phase transitions by simulations and analytical theories can now be compared in detail to experimental results on a microscopic level.

We thank the BMBF for funding via 05K13IPA and 05K12IP1. A. B. thanks the Leibnitz Graduate School “Dynamics in new Light.” We thank Ionela Vrejoiu for preparing the samples as well as Michael Wulff and Dmitry Khakhulin for their invaluable support at the beam line ID9 at the ESRF.

*bargheer@uni-potsdam.de

<http://www.udkm.physik.uni-potsdam.de>

- [1] M. E. Siemens, Q. Li, R. Yang, K. A. Nelson, E. H. Anderson, M. M. Murnane, and H. C. Kapteyn, *Nat. Mater.* **9**, 26 (2010).
- [2] M. N. Luckyanova, J. Garg, K. Esfarjani, A. Jandl, M. T. Bulsara, A. J. Schmidt, A. J. Minnich, S. Chen, M. S. Dresselhaus, Z. Ren, E. A. Fitzgerald, and G. Chen, *Science* **338**, 936 (2012).
- [3] N. Li, J. Ren, L. Wang, G. Zhang, P. Hägggi, and B. Li, *Rev. Mod. Phys.* **84**, 1045 (2012).
- [4] M.-H. Bae, Z. Li, Z. Aksamija, P. N. Martin, F. Xiong, Z.-Y. Ong, I. Knezevic, and E. Pop, *Nat. Commun.* **4**, 1734 (2013).
- [5] M. Maldovan, *Phys. Rev. Lett.* **110**, 025902 (2013).
- [6] J. Ravichandran, A. K. Yadav, R. Cheaito, P. B. Rossen, A. Soukiassian, S. J. Suresha, J. C. Duda, B. M. Foley, C.-H. Lee, Y. Zhu, A. W. Lichtenberger, J. E. Moore, D. A. Muller, D. G. Schlom, P. E. Hopkins, A. Majumdar, R. Ramesh, and M. A. Zurbuchen, *Nat. Mater.* **13**, 168 (2014).
- [7] R. Venkatasubramanian, E. Siivola, T. Colpitts, and B. O’Quinn, *Nature (London)* **413**, 597 (2001).
- [8] B. Poudel, Q. Hao, Y. Ma, Y. Lan, A. Minnich, B. Yu, X. Yan, D. Wang, A. Muto, D. Vashaei, X. Chen, J. Liu, M. S. Dresselhaus, G. Chen, and Z. Ren, *Science* **320**, 634 (2008).
- [9] K. Biswas, J. He, I. D. Blum, C.-I. Wu, T. P. Hogan, D. N. Seidman, V. P. Dravid, and M. G. Kanatzidis, *Nature (London)* **489**, 414 (2012).
- [10] B. Li, L. Wang, and G. Casati, *Phys. Rev. Lett.* **93**, 184301 (2004).
- [11] A. Shukla, M. Calandra, M. d’Astuto, M. Lazzeri, F. Mauri, C. Bellin, M. Krisch, J. Karpinski, S. M. Kazakov, J. Jun, D. Daghero, and K. Parlinski, *Phys. Rev. Lett.* **90**, 095506 (2003).
- [12] O. Delaire, J. Ma, K. Marty, A. F. May, M. A. McGuire, M.-H. Du, D. J. Singh, A. Podlesnyak, G. Ehlers, M. D. Lumsden, and B. C. Sales, *Nat. Mater.* **10**, 614 (2011).
- [13] J. W. L. Pang, W. J. L. Buyers, A. Chernatynskiy, M. D. Lumsden, B. C. Larson, and S. R. Phillpot, *Phys. Rev. Lett.* **110**, 157401 (2013).
- [14] J. Chen, M. Trigo, S. Fahy, D. Murray, Y. M. Sheu, T. Gruber, R. Henning, Y. J. Chien, C. Uher, and D. A. Reis, *Appl. Phys. Lett.* **102**, 181903 (2013).
- [15] M. Trigo, M. Fuchs, J. Chen, M. P. Jiang, M. Cammarata, S. Fahy, D. M. Fritz, K. Gaffney, S. Ghimire, A. Higginbotham, S. L. Johnson, M. E. Kozina, J. Larsson, H. Lemke, A. M. Lindenberg, G. Ndabashimiye, F. Quirin, K. Sokolowski-Tinten, C. Uher, G. Wang *et al.*, *Nat. Phys.* **9**, 790 (2013).
- [16] M. Först, C. Manzoni, S. Kaiser, Y. Tomioka, Y. Tokura, R. Merlin, and A. Cavalleri, *Nat. Phys.* **7**, 854 (2011).
- [17] F. Rollins, *Appl. Phys. Lett.* **2**, 147 (1963).
- [18] P. J. S. van Capel and J. I. Dijkhuis, *Appl. Phys. Lett.* **88**, 151910 (2006).
- [19] A. Bojahr, M. Herzog, D. Schick, I. Vrejoiu, and M. Bargheer, *Phys. Rev. B* **86**, 144306 (2012).
- [20] O. L. Muskens and J. I. Dijkhuis, *Phys. Rev. Lett.* **89**, 285504 (2002).
- [21] W. Singhsomroje and H. J. Maris, *Phys. Rev. B* **69**, 174303 (2004).
- [22] E. Péronne and B. Perrin, *Ultrasonics* **44**, e1203 (2006).
- [23] A. Bojahr, M. Herzog, S. Mitzscherling, L. Maerten, D. Schick, J. Goldshteyn, W. Leitenberger, R. Shayduk, P. Gaal, and M. Bargheer, *Opt. Express* **21**, 21188 (2013).
- [24] D. Schick, M. Herzog, A. Bojahr, W. Leitenberger, A. Hertwig, R. Shayduk, and M. Bargheer, *Struct. Dyn.* **1**, 064501 (2014).
- [25] C. Klieber, E. Peronne, K. Katayama, J. Choi, M. Yamaguchi, T. Pezeril, and K. A. Nelson, *Appl. Phys. Lett.* **98**, 211908 (2011).
- [26] M. Herzog, A. Bojahr, J. Goldshteyn, W. Leitenberger, I. Vrejoiu, D. Khakhulin, M. Wulff, R. Shayduk, P. Gaal, and M. Bargheer, *Appl. Phys. Lett.* **100**, 094101 (2012).
- [27] R. Shayduk, M. Herzog, A. Bojahr, D. Schick, P. Gaal, W. Leitenberger, H. Navirian, M. Sander, J. Goldshteyn, I. Vrejoiu, and M. Bargheer, *Phys. Rev. B* **87**, 184301 (2013).
- [28] See Supplemental Material at <http://link.aps.org/supplemental/10.1103/PhysRevLett.115.195502> for details of the experimental setups, the data analysis and theory, which includes Refs. [29–36].
- [29] N. Li and B. Li, *Europhys. Lett.* **78**, 34001 (2007).
- [30] C. Alabiso, M. Casartelli, and P. Marenzoni, *J. Stat. Phys.* **79**, 451 (1995).
- [31] J. Liu, S. Liu, N. Li, B. Li, and C. Wu, *Phys. Rev. E* **91**, 042910 (2015).
- [32] C. Herring, *Phys. Rev.* **95**, 954 (1954).
- [33] H. J. Maris, *Phys. Acoust.* **8**, 279 (1971).
- [34] H. Y. Hao and H. J. Maris, *Phys. Rev. B* **64**, 064302 (2001).
- [35] A. N. Cleland, *Foundations of Nanomechanics: From Solid-State Theory to Device Applications*, Advanced Texts in Physics and Astronomy (Springer, Berlin, 2003).
- [36] G. P. Berman and F. M. Izrailev, *Chaos* **15**, 015104 (2005).
- [37] P. Gaal, D. Schick, M. Herzog, A. Bojahr, R. Shayduk, J. Goldshteyn, H. A. Navirian, W. Leitenberger, I. Vrejoiu, D. Khakhulin, M. Wulff, and M. Bargheer, *J. Synchrotron Radiat.* **21**, 380 (2014).
- [38] L. Maerten, A. Bojahr, M. Gohlke, M. Rössle, and M. Bargheer, *Phys. Rev. Lett.* **114**, 047401 (2015).
- [39] C. Thomsen, H. T. Grahn, H. J. Maris, and J. Tauc, *Phys. Rev. B* **34**, 4129 (1986).
- [40] M. Bradler, P. Baum, and E. Riedle, *Appl. Phys. B* **97**, 561 (2009).
- [41] S. Lepri, R. Livi, and A. Politi, *Phys. Rev. Lett.* **78**, 1896 (1997).
- [42] B. Gershgorin, Y. V. Lvov, and D. Cai, *Phys. Rev. Lett.* **95**, 264302 (2005).
- [43] N. Li, P. Tong, and B. Li, *Europhys. Lett.* **75**, 49 (2006).
- [44] S. Liu, J. Liu, P. Hägggi, C. Wu, and B. Li, *Phys. Rev. B* **90**, 174304 (2014).
- [45] E. L. Meeks and R. T. Arnold, *Phys. Rev. B* **1**, 982 (1970).
- [46] A. Bojahr, D. Schick, L. Maerten, M. Herzog, I. Vrejoiu, C. von Korff Schmising, C. J. Milne, S. L. Johnson, and M. Bargheer, *Phys. Rev. B* **85**, 224302 (2012).
- [47] R. L. Bivins, N. Metropolis, and J. R. Pasta, *J. Comput. Phys.* **12**, 65 (1973).
- [48] D. Sholl, *Phys. Lett. A* **149**, 253 (1990).